International Journal of Automotive Technology, Vol. 8, No. 6, pp. 687–696 (2007)

1229-9138/2007/037-03

EFFECT OF VALVE TIMING AND LIFT ON FLOW AND MIXING CHARACTERISTICS OF A CAI ENGINE

J. N. KIM[1], H. Y. KIM[1]*, S. S. YOON[1], S. D. SA[1] and W. T. KIM[2]

[1]Department of Mechanical Engineering, Korea University, Seoul 136-713, Korea
[2]Hyundai Motor Company, 772-1 Jangdeok-dong, Hwaseong-si, Gyeonggi 445-706, Korea

(Received 12 July 2007; Revised 14 September 2007)

ABSTRACT–To increase the reliability of auto-ignition in CAI engines, the thermodynamic properties of intake flow is often controlled using recycled exhaust gases, called internal EGR. Because of the internal EGR influence on the overall thermodynamic properties and mixing quality of the gases that affect the subsequent combustion behavior, optimizing the intake and exhaust valve timing for the EGR is important to achieve the reliable auto-ignition and high thermal efficiency. In the present study, fully 3D numerical simulations were carried out to predict the mixing characteristics and flow field inside the cylinder as a function of valve timing. The 3D unsteady Eulerian-Lagrangian two-phase model was used to account for the interaction between the intake air and remaining internal EGR during the under-lap operation while varying three major parameters: the intake valve (IV) and exhaust valve (EV) timings and intake valve lift (IVL). Computational results showed that the largest EVC retardation, as in A6, yielded the optimal mixing of both EGR and fuel. The IV timing had little effect on the mixing quality. However, the IV timing variation caused backflow from the cylinder to the intake port. With respect to reduction of heat loss due to backflow, the case in B6 was considered to present the optimal operating condition. With the variation of the intake valve lift, the A1 case yielded the minimum amount of backflow. The best mixing was delivered when the lift height was at a minimum of 2 mm.

KEY WORDS : CAI (Controlled Auto Ignition), Under-lap, Internal EGR (Exhaust Gas Recirculation), Uniformity

1. INTRODUCTION

Controlled auto ignition (CAI) or homogeneous charge compression ignition (HCCI) is considered one of the most advanced combustion modes among numerous types of internal combustion engines due to its merits over other conventional spark ignition (SI) and compression ignition (CI) modes. The term "auto-ignition" refers to natural ignition without a spark when a certain critical pressure or temperature is exceeded due to the compression within the combustion cylinder.

In the CAI engine, however, there is no direct method to control auto-ignition timing. Hence, the ignition mechanism is specified by the operating parameters, such as fuel properties, intake air temperature, A/F ratio, intake port and exhaust port pressures, fuel injection time and engine speed. Furthermore, the ignition time is also influenced by the engine "performance" parameters, such as the internal EGR rate, valve timing and compression ratio. Through a clever handling of these aforementioned parameters, auto-ignition timing can be optimized to render a rapid and stable combustion mode to achieve higher overall efficiency and reduce the emission level of environmentally hazardous gases.

The combustion temperature of CAI engines is generally found to be significantly lower than that of SI engines. As a result, the NOx emission level of CAI engines is substantially lower than that of SI engines; therefore, CAI engines are preferable over SI engines. However, poor mixing or stratification between fuel and intake gases often poses a great technical challenge, which prevents the improvement of the CAI engine. Due to the gas mixture stratification, incomplete combustion is often induced, yielding high emission levels of environmentally hazardous gases such as HC and CO. The emission levels of these gases can be, sometimes, higher than those of SI engines. Thus, optimizing the operating condition of the CAI engine is necessary.

Nowadays, in the automobile industry, the mixture stratification issue can be circumvented by optimizing the intake and exhaust valve timings of the CAI engine. Furthermore, optimizing the valve timings is crucial because of its critical effect on the auto-ignition mechanism.

The use of high volatile fuels, like hydrogen and ethanol, is favorable in achieving better mixing with other gases

*Corresponding author. e-mail: kimhy@korea.ac.kr

Table 1. Generalized equation.

	Equation	φ	Γ_φ	S_φ
Continuous phase	Continuity	1	0	$S_{d,m}$
	Momentum	u_i	μ_e	$-\frac{\partial p}{\partial x_i}+\frac{\partial}{\partial x_j}\left(\mu_e\frac{\partial u_j}{\partial x_i}-\frac{2}{3}\left(\rho k+\mu_t\frac{\partial u_k}{\partial x_k}\right)\delta_{ij}\right)+S_{d,u_i}$
	Turbulent kinetic energy	k	$\mu+\frac{\mu_t}{\sigma_k}$	$G_k-\rho\varepsilon$
	Dissipation rate	ε	$\mu+\frac{\mu_t}{\sigma_\varepsilon}$	$\frac{\varepsilon}{k}(c_1G_k-c_2\rho\varepsilon)$
	Species	Y_s	$\frac{\lambda}{C_p}+\frac{\mu_t}{\sigma_Y}$	$S_{d,j}$
	Energy	h	$\frac{\lambda}{C_p}+\frac{\mu_t}{\sigma_h}$	$S_{d,h}$

where, $G_k=\mu_t\left(\frac{\partial u_i}{\partial x_j}+\frac{\partial u_j}{\partial x_i}\right)\frac{\partial u_j}{\partial x_i}$, $\mu_e=\mu+\mu_t$, $\mu_t=\rho c\frac{k^2}{\varepsilon}$ and σ_φ: Turb. Prantle No.

(Sato *et al.*, 2006); however, this choice necessitates the cumbersome implementation of extraneous fuel supply systems or additives.

The intake air temperature has a prominent influence on the fuel ignition time. If the intake air temperature is increased, ignition can be achieved sooner. However, the practical application of increasing intake air temperature limited by the extra cost involved with installing a large volume heater. In addition, limitations on the operating range are an additional source of concern when using the large volume heater, which also causes low volumetric efficiency (Aoyama *et al.*, 1996; Christensen *et al.*, 1997, 1998). Christensen *et al.* (1999) investigated the effect of various compression ratios on NOx emission and combustion instability and showed that the NOx emission decreased when the intake air temperature was lowered at a relatively high compression ratio. However, their suggested design seems to be impractical because of the complex design and high production cost.

From a practical point of view, taking advantage of the high temperature of the residual gas trapped inside the combustion cylinder seems to be economically the most viable way to achieve auto-ignition of the CAI engine, the facilitation of which would require a VVT (variable valve timing) or VVA (variable valve actuation). Residual gases are trapped by early exhaust valve closure, referred to as NVO (negative valve overlap or often referred to as "under-lap" period) (Li *et al.*, 2001; Lavy *et al.*, 2000), and re-circulation of the hot exhaust gases, fed back into the intake stroke by late exhaust valve closure, referred to as the "large valve overlap".

The objective of the current work is to numerically examine the effects of valve timing and lift on the mixing characteristics (or homogeneity) of residual gases, intake air, and fuel during the negative valve overlap motion. Distinguished from other CAI engine research, this research quantifies the aforementioned effects.

All numerical simulations were performed by using the 3D unsteady Eulerian Navier-Stokes solvers, coupled with the Lagrangian particle tracking model to the spray dynamics. Mixing characteristics without ignition are considered in the current study. Thus, the optimal mixing condition suggested herein is applicable for the gas mixing process and may not guarantee optimal performance for processes that include ignition and subsequent combustion.

2. SIMULATION

2.1. Governing Equation

The conservation equations for continuous phase can be described by Equation (1) with the variables given in Table 1.

$$\frac{\partial}{\partial t}(\rho\varphi)+\frac{\partial}{\partial x_j}(\rho u_j\varphi)=\frac{\partial}{\partial x_j}\left(\Gamma_\varphi\frac{\partial\varphi}{\partial x_j}\right)+S_\varphi \tag{1}$$

When liquid fuel is injected, the droplet velocity and displacement, u_{di} and x_{di} can be expressed by Newton's 2nd law of motion:

$$m_d\frac{du_{di}}{dt}=\frac{1}{2}C_D\rho A_d|u_i-u_{di}|(u_i-u_{di})-V_d\nabla p \tag{2}$$

$$\frac{dx_{di}}{dt}=u_{di} \tag{3}$$

where, the drag coefficient, C_D, is estimated by the correlation of Yuen and Chen (1976).

The heat and mass transfer of a single droplet are calculated by using the conservation of mass and energy:

$$\frac{dm_d}{dt} = -A_s K_g p_t \ln\frac{(p_t - p_{v,\infty})}{(p_t - p_{v,s})} \quad (4)$$

$$m_d \frac{d(c_{p,d} T_d)}{dt} = -A_s h(T_d - T) + h_{fg}\frac{dm_d}{dt} \quad (5)$$

Here, K_g and h represent the mass and heat transfer coefficients, respectively, which can be obtained from the Ranz-Marshall relation (1952). As for the atomization model, the primary and secondary atomization models of Reitz and Diwakar (Reitz and Diwakar, 1986; Nicholls, 1972) were utilized.

2.2. Grid Generation

The engine has a bore of 88 mm and a stroke of 97 mm. The compression ratio is 10.5:1. The cylinder head features a centrally mounted fuel injector and a pent roof combustion chamber. Obtained using *Pro-am* and *ES-ICE*, an adaptive moving grids reflecting the computational domain changes with time due to the moving parts (i.e., intake valve, exhaust valve and piston), were constructed. Figure 1 shows the constructed grids for the CAI engine used in the current study. When the piston is at the TDC (Top Dead Center), the grid resolution began with approximately 320,000 nodes and increased to about 700,000 nodes at the BDC (Bottom Dead Center).

2.3. Parametric Studies and Numerical Details

Table 2 lists a total of 13 cases considered in the current parametric studies. The upper and lower Tables show the variation in EVO/EVC and IVO/IVC, respectively. Case "A1" is the benchmarking case. In the upper table, the EVO timing was varied from 140 to 120 CAD under the fixed EVC for cases A1, A2, and A3. For cases A4, A5, and A6, EVC was varied from 300 to 320 CAD under a constant EVO. Because NVO represents the period between the EVC and IVO, the NVO timing was accordingly shifted from 140 to 120 CAD during the EVC variation. The cases in the lower table were constructed similarly to examine the effects of IVO/IVC timings and NVO.

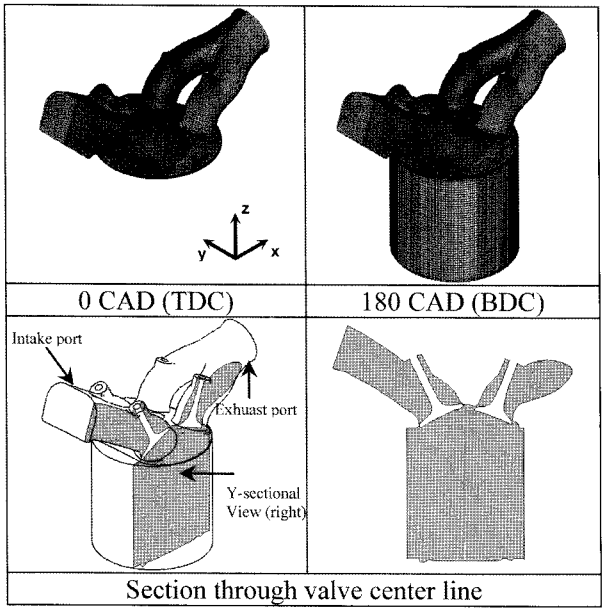

Figure 1. Generated grids for various crank angle and schematics.

Table 2. Operating condition for the CAI engine.

Exhaust valve timing						
	A1	A2	A3	A4	A5	A6
EVO	140	130	120	140	140	140
EVC	290	290	290	300	310	320
IVO	440	440	440	440	440	440
IVC	590	590	590	590	590	590
NVO	150	150	150	140	130	120

Intake valve timing								
	A1	B1	B2	B3	B4	B5	B6	B7
EVO	140	140	140	140	140	140	140	140
EVC	290	290	290	290	290	290	290	290
IVO	440	430	420	440	440	440	420	460
IVC	590	590	590	600	610	620	570	610
NVO	150	140	130	150	150	150	130	170

Additional parametric studies with variation of the intake valve lift were also performed. The intake valve lift is the perpetual shaft, which allows the flow of the intake air into the cylinder. Depending on the lift depth (or height), the flow speed at the intake port can be controlled.

Figure 2 shows the intake valve lift varying with time

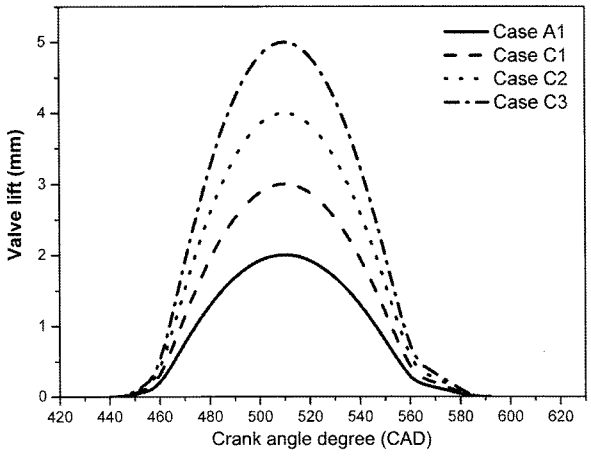

Figure 2. Intake valve lift for each case.

Table 3. Wall temperature condition.

Cylinder wall	400 K	Piston head	520 K
Cylinder head	520 K	Valve head	800 K

or crank angle. The maximum valve lift reaches 2, 3, 4, and 5 mm for cases A1, C1, C2, and C3, respectively. Higher speeds due to flow acceleration are expected when the valve lift is small.

As for the boundary conditions, the pressure at the intake and exhaust port was fixed to the standard atmospheric pressure (for boost system with turbo or supercharger); thus, velocities were extrapolated at both ports. No-slip wall boundary conditions were applied to all solid surfaces.

Table 3 shows the temperature condition at every component of the CAI engine. The properties of a monocomponent gas were assumed for the exhaust gas (e.g., the gas comprises N_2, H_2O, CO_2, CO, H_2 and O_2) to be consistent with the previously obtained data (private communications with Hyundai Motor Company).

To solve the flow field, the PISO algorithm (Issa, 1986) was coupled with MARS (Monotone Advection and Reconstruction Scheme), whose accuracy is minimally affected by the skewness in mesh structure (Asproulis, 1994). The standard RANS (Reynolds Averaged Navier Stokes) $k-\varepsilon$ model was used for turbulence. Beginning at 0 CAD, the duration of the numerical simulation reached 720 CAD, during which 2 revolutions of the crank-piston cycles are completed. This time duration necessitated 3600 time steps at Δt = 0.2 CAD.

3. RESULTS AND DISCUSSION

3.1. Effect of Exhaust Valve Timing

Figure 3 shows the histories of the pressure inside the cylinder for various EV timings (A1–A6 cases). The time or the crank angle from 120 to 720 degrees comprised the exhaust stroke, negative valve overlap (sometimes referred to as the "re-compression" stroke), intake and compression stroke. Because of the nature of CAI engines (e.g., taking advantage of high re-compression pressure for auto-ignition), the peak gas pressure inside the cylinder occurred during the time range known as NVO or simply "under-lapping." The pumping loss, which is a typical in the overlapping engine, can be reduced in the under-lapping CAI engine by the high pressure of the residual gases.

As shown, the peak pressure of A4, A5, and A6 cases decreased when the EVC timing was retarded (or extended). The result is due to the smaller amount of residual gases remaining inside the cylinder as a result of the increased amount of exiting gases with more retarded

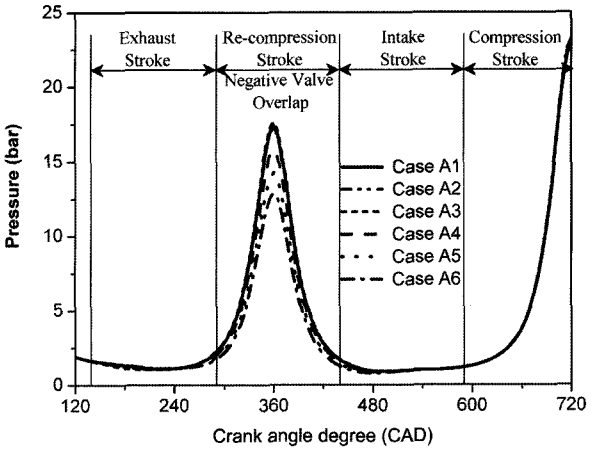

Figure 3. Cylinder pressure for various exhaust valve timings.

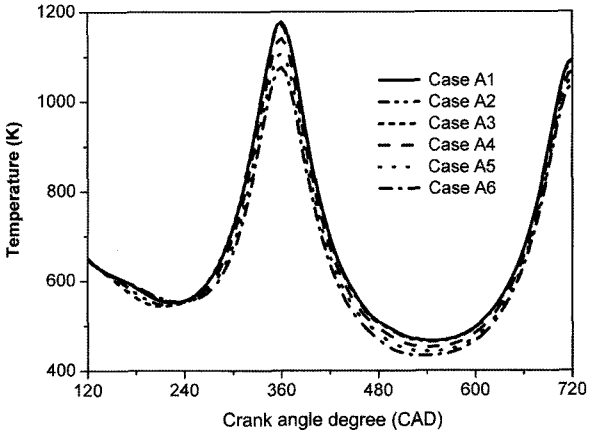

Figure 4. Cylinder temperature for various exhaust valve timings.

EVC timing. However, toward the end of the compression stroke at 720 CAD, all cases reached the same pressure because the low and high pressure cylinders were adjusted with large and small intake air flow, respectively, during the intake stroke.

Figure 4 shows the cylinder's temperature as it varies with time. When the EVC timing was retarded, more residual gases were removed or exhausted. Because the cylinder's low pressure induced a larger infiltration of the intake air of low temperature, the cylinder temperature decreased.

Figure 5 shows the mass concentration of the internal EGR inside the cylinder, the time range of which included the intake and compression stroke. When the EVC timing was retarded (allowing the larger supply of the intake air) as in cases A4–A6, the EGR mass concentration inside the cylinder decreased. The cases A1–A3, having relatively high cylinder pressure under fixed EVC, showed the same start-off point for the intake

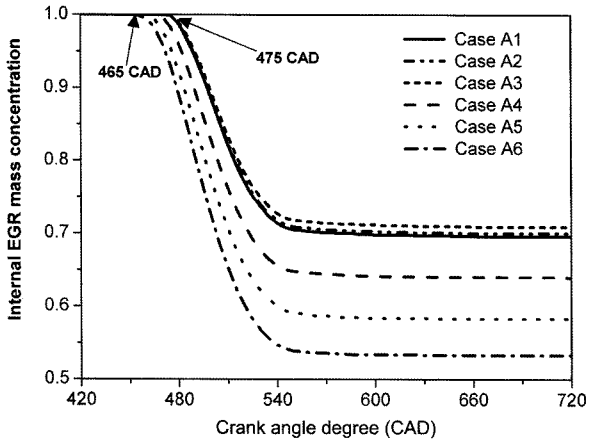

Figure 5. Mass concentration of internal EGR inside cylinder for various exhaust valve timings.

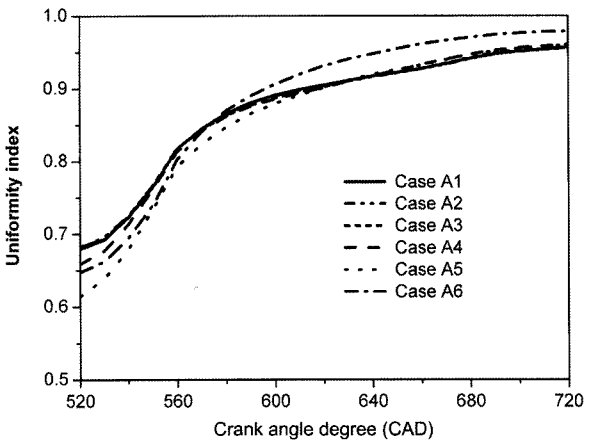

Figure 6. Uniformity index of internal EGR for various exhaust valve timings.

stroke, approximately at 475 CAD. For these high pressure cases, backflow from the cylinder to the intake port occurred, and the initiation of the intake stroke was delayed. However, as for cases A4–A6, the start-off point was slightly expedited because of the extended EVC, which yielded a more favorable intake stroke environment with relatively low cylinder pressure.

Figure 6 shows the uniformity of the internal EGR at various exhaust valve timings; at 520 CAD, the intake stroke was completed and the compression stroke continued increasing until 720 CAD.

The uniformity index, η, is defined as follows (Weltens, 1993):

$$\eta = 1 - \sum_{i=1}^{n} \frac{|C_i - \bar{C}| V_i}{2\bar{C}V} \tag{4}$$

where, C_i and $\bar{C}$ are the local and average EGR mass concentrations, V_i and $\bar{V}$ are the local and average volume, respectively. The internal EGR mass concentration and the volume at every cell were used for the η definition. A higher uniformity index is indicative of a more homogeneous mixing. Toward the end of the compression stroke (at about 720 CAD), the uniformity index of the internal EGR for the case A6 reached approximately 0.98 while those of the other cases were near 0.96. Because the EVC of case A6 was retarded (or extended) by 30 CAD with respect to the benchmark case A1, a larger amount of the intake air induced vigorous mixing between the internal EGR and the intake air, resulting in better mixing at a higher uniformity index value. Figure 7 shows the flow field snapshots of the valve center at 515 CAD, the instant at which the intake valve was fully opened. As for case A6, the EVC retardation was at maximum (320 CAD), leading to the largest pressure difference between the cylinder pressure (lowest, as shown in Figure 3) and the constant intake port pressure (1 bar). Thus, the largest amount of intake air was supplied. This largest mass flow rate caused maximum penetration and vigorous mixing. This result is in contrast with cases A1–A5 (Figure 7).

The snapshots shown in Figure 8 indicate the mass concentration of the internal EGR during the compression stroke (both intake and exhaust valves were closed). Case A6 seemed to have the optimal mixing of the internal EGR and intake air because it had the largest mass flow rate. For cases A2 and A3, the mixing characteristics never seemed to improve despite the EVO advancement, which is the opposite of EVC retardation (Table 2). This change in EVO timing seemed to have

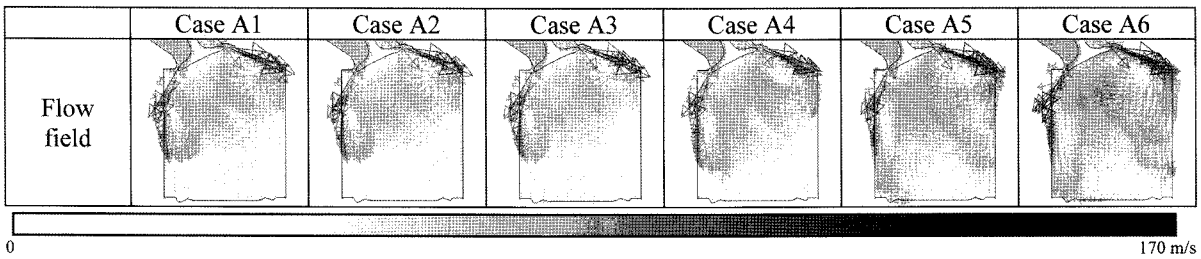

Figure 7. Flow field at intake valve fully opened in the section of valve center.

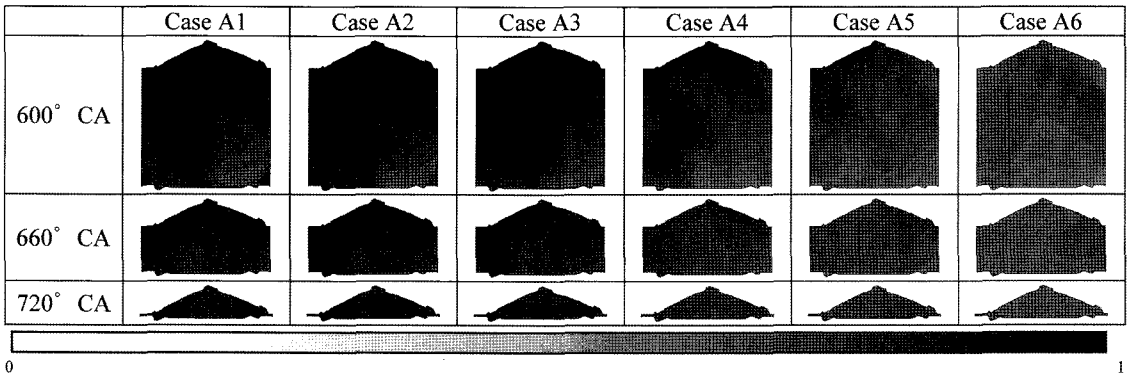

Figure 8. Mass concentration of internal EGR during compression stroke.

little effect on the flow characteristics, based on our observation from Figures 3-8.

The mixing characteristics of the evaporated fuel have a great influence on CAI engine performance. When the gas mixture is stratified, the region with dense fuel vapor is readily ignited, and a larger portion of the mixture having dilute fuel vapor will be secondarily ignited by the primarily ignited flame. This reaction triggers a cyclic unbalance. This type of mixture stratification slows the reaction rate and, thus, induces relatively low combustion pressure and temperature. These sequential processes also, in turn, render incomplete combustion, producing HC and CO, environmentally hazardous gases. On the other hand, when the mixture is homogeneous, the combustion kinetics becomes faster and more stable, so a higher overall efficiency is obtained in addition to lower levels of HC and CO emissions, even though more frequent knockings and higher NOx emission level may be produced (Li *et al.*, 2006) compared to the heterogeneous mixing cases. The NOx emission of the CAI engine is far less than that of other conventional engine types, such as SI or CI engines.

We examined the influence of the EVC retardation on fuel mixing, as shown in Figure 9. The results were obtained at various instants (e.g., at 600, 660, and 720 CAD) for cases A1, A4, A5, and A6. The fuel was injected at the top center of the combustion dome for a duration of 2 ms, which was equivalent to 24 CAD at the given 2000 rpm, 2 bar bmep of operating condition. The fuel, iso-octaine, was injected during the re-compression stroke ($348 < t_{inj} < 372$ CAD) for rapid fuel evaporation and stable auto-ignition.

For all these cases in Figure 9, the injected fuel was quickly entrained by the intake air, so a vortical motion was formed in the clockwise direction. Because of the strong momentum of the intake air in the upper left corner, fuel was pushed toward the bottom right corner, resulting in high fuel concentration in that region. Toward the end of the compression stroke (720 CAD), case A6

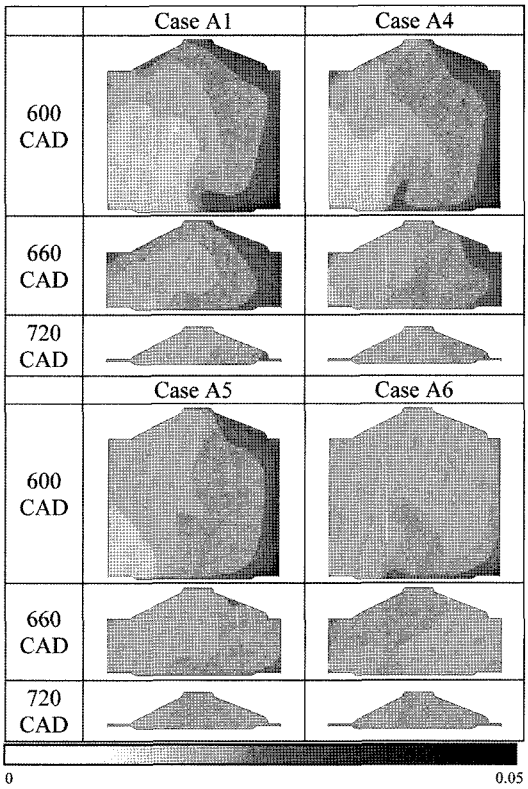

Figure 9. Mass concentration of evaporated fuel during compression stroke.

showed the most homogeneous mixing of the fuel; this result is consistent with that shown in Figure 10. The fuel uniformity index of the case A6 was the highest among the compared cases. Moreover, case A6 yielded the best homogeneous mixing condition for the EGR also (see Figure 6), and this trend was similar to that of the fuel shown in Figure 10.

However, the difference in η between cases A1 and A6 of Figure 10 was far greater than that shown in Figure 6. This greater margin in $\Delta\eta$ implied that the fuel mixing

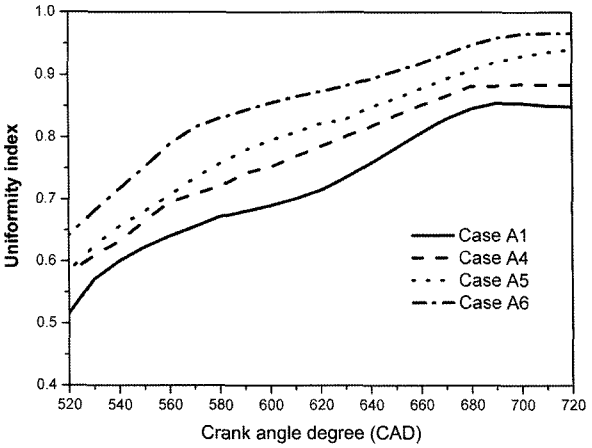

Figure 10. Uniformity index of evaporated fuel.

was more readily influenced by the intake air condition compared to the EGR. Based on these observations, we deduced that case A6 presented the most optimal condition for subsequent combustion, not because of the well mix of EGR (see Figure 6), but because of the well mix of fuel (Figure 10).

3.2. Effect of Intake Valve Timing

In this section, the effect of the intake valve timing is examined and discussed. The parametric variations of IVO and IVC are listed in Table 2.

Figure 11 shows the history of the cylinder's pressure for various cases (A1 and B1–B7). The time from 120 to 720 CAD comprised the exhaust stroke, negative valve overlap, intake stroke and compression stroke. As shown, the intake valve timing had practically no effect on the pressure while the exhaust valve time had a great influence on the pressure (see Figure 3). Consequently, all other mixing characteristics (such as cylinder temperature,

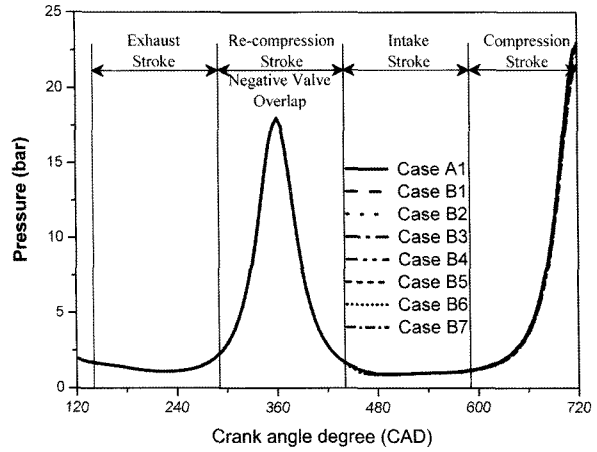

Figure 11. Cylinder pressure for various intake valve timings.

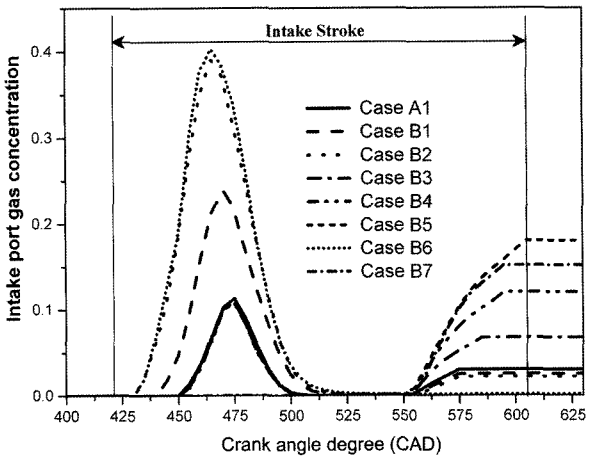

Figure 12. Mass concentration of internal EGR in intake port for various intake valve timings.

η and flow fields) also remained unchanged.

However, the appearance of backflow was observed, similar to the cases with varying exhaust valve timing in the previous section. This backflow can negatively affect the CAI combustion behavior because of the following reasons: firstly, the injected fuel can be caught in the backflow stream and be ejected outside the cylinder and secondly, the backflow may result in substantial heat loss because of hot gases being ejected outside the cylinder.

Figure 12 shows the mass concentration of the gases inside the intake port, which contained air and the backflowed EGR. The range of the crank-angle (400~625 degrees) indicates the intake stroke, which followed the re-compression stroke. It should be noted that occurrence of backflow was caused by the cylinder pressure being temporarily greater than the intake port pressure. There are two dominant temporal increases in the intake port gas concentration, as shown in Figure 12. The first increase is the Gaussian-shaped peak, commonly referred to as the "early-backflow". The second peak occurs in the flattening curve, commonly referred to as the "late-backflow".

For the early-backflow, the intake port gas concentrations of cases B2 and B6 were shown to have the highest values because of the most advanced IVO (e.g., IVO=420 from Table 2), allowing the largest amount of backflow among all cases (see the gas concentration contour plots of Figure 13 in conjunction with Figure 12). When IVO=430, the concentration was approximately 0.24, which was the same in case B1. When the IVO timing was further retarded (IVO=440) as in cases A1 and B3–B5, the concentration level was relatively small because of sufficient expansion, which further reduced the cylinder pressure. In this case, the cylinder pressure causing backflow to the intake port was not sufficient. For qualitative comparison, see the corresponding contour

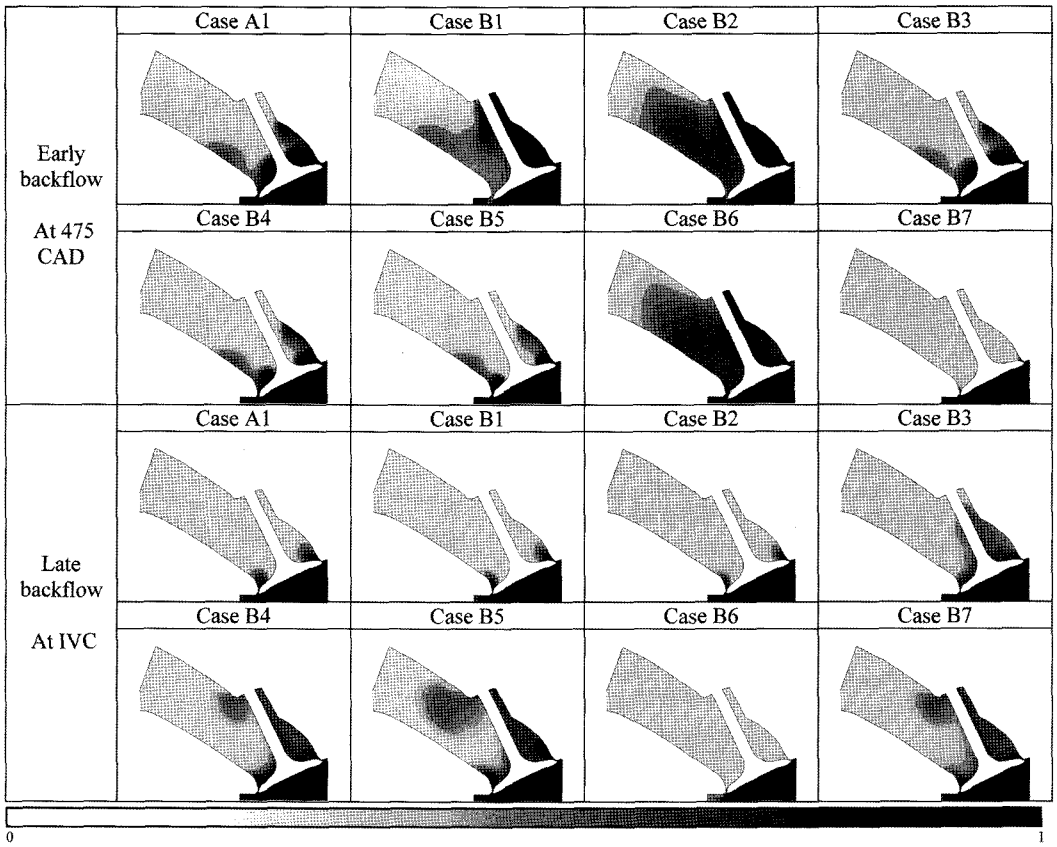

Figure 13. Early and late backflow pattern for various intake valve timing.

plots in Figure 13. For case B7, backflow was never induced because of the most retarded IVO=460, which rendered the lowest cylinder pressure. This low pressure did not cause backflow of the EGR into the intake port.

For late-backflow, the trend was different from that shown for early-backflow. While early-backflow was strongly affected by IVO, late backflow was not. Rather, late backflow was strongly affected by IVC. When IVC=620 was at the most retarded, as in case B5 (which physically means the late closing of the intake valve), late-backflow was also the largest. When IVC was advanced to IVC=610, the gas concentrations of cases B7 and B4 were 0.15 and 0.12, respectively. This trend seemed counter-intuitive, based on the given more retarded IVO=460 of B7 than IVO=440 of B4. Typically, when IVO is retarded, less backflow should be observed due to the smaller exposure (or opening) period of the intake port to the cylinder. To explain this counter-intuitive trend, the effective IVO of B4 was rather 475 (see Figure 12), not 440, which was the originally specified IVO timing. Because of this more retarded effective IVO of B4, a smaller supply of intake air and reduced cylinder pressure were induced before IVC timing. At the most advanced IVC=590, as in cases A1, B1, and B2, late backflow was at a minimum (Figure 12).

With respect to improvement of thermal efficiency, the case yielding the smallest heat loss was identified. The heat loss due to early-backflow is not of major concern since the back-flowed EGR are pushed back into the cylinder by the intake air. However, the heat loss due to late-backflow is unfavorable because of the longer residence period of the hot EGR in the intake port; this EGR is trapped inside the intake port until the next cycle. For this reason, the case without late-backflow, such as case B6, presents the most optimal operating condition in terms of improved thermal efficiency.

3.3. Effect of Intake Valve Lift

In the previous sections 3.1 and 3.2, the effects of exhaust and intake valve timings, respectively, were examined for constant valve lift (2 mm). In this section, the effects of the intake valve lift on gas mixing and thermal characteristics are discussed. For our parametric studies, we changed the intake valve lift from 2 mm to 5 mm by an increment of 1 mm, as mentioned earlier in Figure 2.

Figure 14 shows the gas speed contour for cases A1, C1, C2 and C3 at the instant of maximum valve lift, approximately at 515 CAD. When the intake valve lift

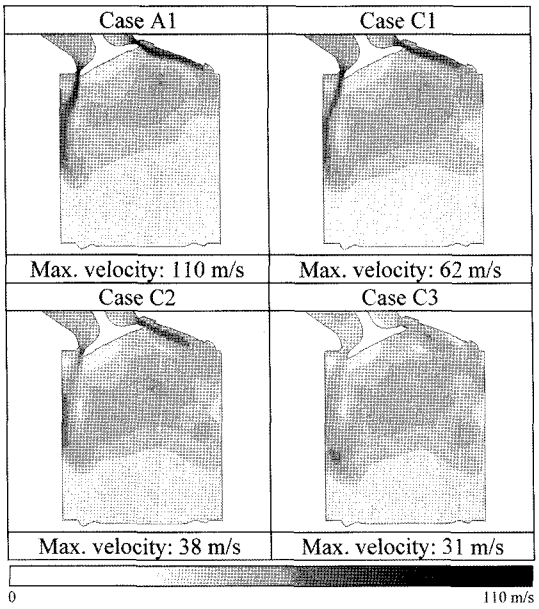

Figure 14. Flow field at maximum valve lift.

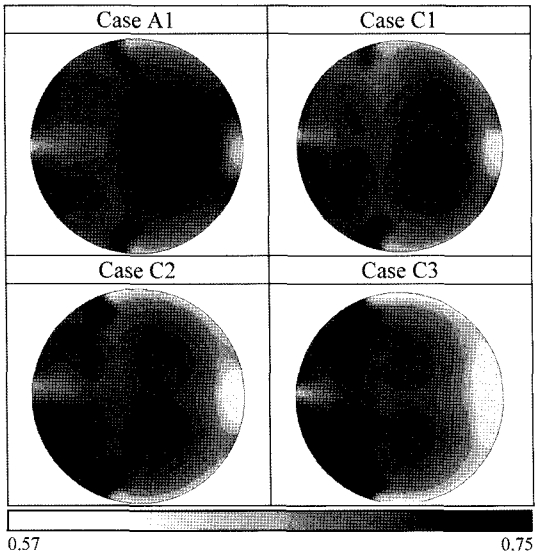

Figure 15. Mass concentration of internal EGR across the combustion chamber at BTDC 10 CAD (equivalent to 710 CAD).

was increased, greater flow penetration seemed to occur because of larger mass flow (or larger discharge coefficient). Though the inlet pressure was fixed, because of the larger area through which the intake air was passing, larger mass flux was induced at the given larger valve lift. However, the mixing quality (or homogeneity), as in case A1, seems to be the most optimal, as shown in Figure 15. Note that case A1 was conduckted with the smallest valve lift. The snapshots were taken at BTDC 10 CAD, the time at which auto-ignition was presumed to occur.

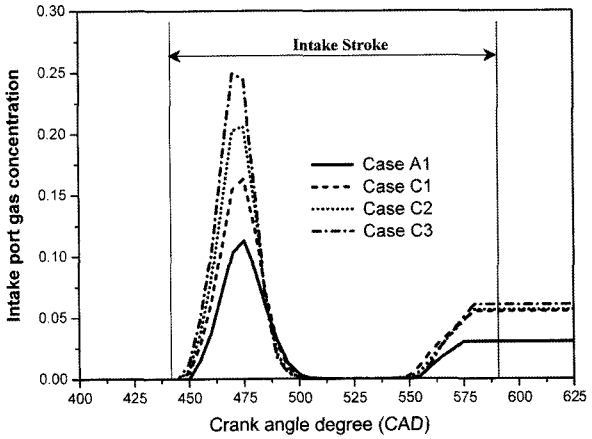

Figure 16. Mass concentration of internal EGR in intake port for various intake valve lifts.

In IC-engines, there are two typical vortices motions, known as, "tumbling" and "swirling." These refer to the vortical motion in the z-x plane (see Figure 14) and the x-y plane (see Figure 15), respectively. Case A1 showed the greatest tumbling motion among all cases (which may not seem very obvious in Figure 14, showing snapshots taken at 540 CAD) while case C3 showed the greatest swirling motion, as shown in Figure 15. When the valve lift decreased (i.e., C3 → A1), the swirling motion was certainly weakened. While decreasing the valve lift, the flow acceleration at the intake port down-end increased. This increase in flow acceleration introduced a stronger tumbling motion in the z-x plane within the cylinder, which, in turn, tended to yield better mixing.

Figure 16 shows the intake port gas concentration during the intake stroke over the time range of 440~590 CAD. The early and late backflows occurred from 450~510 CAD and 550~580 CAD, respectively. While increasing the intake valve lift (i.e., A1 → C3), higher gas concentration inside the intake port was observed for both early and late backflows. The gas concentration was increased by increments of 0.05, 0.04, and 0.03 with respect to 50, 33, and 25% change in the valve lift. The qualitatively data of this trend are shown in Figure 17.

Case A1 yielded the least amount of backflow during the intake stroke. Furthermore, best mixing was achieved with a 2 mm valve lift. This result supports our justification in choosing case A1 as presenting the optimal operating condition.

4. CONCLUSION

Because of the internal EGR influence on the overall thermodynamic properties and mixing quality of the gases inside a combustion cylinder, optimizing the intake and exhaust valve timings is important to achieve reliable

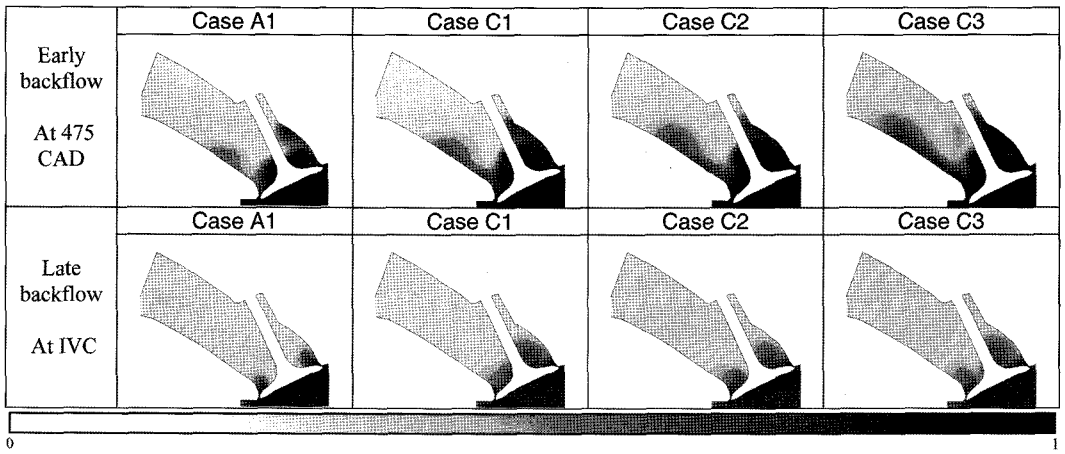

Figure 17. Early and late backflow pattern for various intake valve lift.

auto-ignition and high thermal efficiency. Fully 3D numerical simulations were performed to predict the mixing characteristics and flow field inside the cylinder as a function of various valve timings. To account for the interaction between the intake air and the remaining internal EGR for the CAI engine, three major parameters were varied: the intake valve (IV) and exhaust valve (EV) timings and intake valve lift (IVL). Computational results showed that the largest EVC retardation as in case A6 yielded the most optimal mixing of both EGR and fuel. The IV timing had little effect on the mixing quality. However, the IV timing variation caused backflows from the cylinder to the intake port. With respect to the reduction of heat loss due to backflow, case B6 was considered to present the most optimal operating condition. With the variation of the intake valve lift, case A1 yielded the least amount of backflow. The best mixing was delivered when the lift height was at minimum of 2 mm.

ACKNOWLEDGEMENT–This research was supported by a grant from Development of Engine System for HEV Project, funded by the Ministry of Commerce, Industry and Energy.

REFERENCES

Asproulis, P. N. (1994). *High Resolution Numerical Predictions of Hypersonic Flows on Unstructured Meshes.* Ph. D. Dissertation. Imperial College. England.

Aoyama, T., Hattori, Y. and Mizuta, J. (1996). An experimental study on premixed-charged compression ignition gasoline engine. *SAE Paper No.* 960081.

Christensen, M., Hohansson, B. and Einewall, P. (1997). Homogeneous charge compression ignition (HCCI) using isooctane, ethanol and natural gas-A comparison with spark ignition operation. *SAE Paper No.* 972874.

Christensen, M. and Hohansson, B. (1998). Influence of mixture quality on homogeneous charge compression ignition. *SAE Paper No.* 982454.

Christensen, M., Hultqvist, A. and Hohansson, B. (1999). Demonstrating the multi fuel capability of a homogeneous charge compression ignition engine with variable compression ratio. *SAE Paper No.* 1999-01-3679.

Issa, R. I. (1986). Solution of the implicitly discretised fluid flow equations by operator-splitting. *J. Comp. Phys.*, **62**, 40–65.

Lavy, W., Dabadie, J., Willand, J., Juretzka, A., Ma, T., Lendresse, Y., Schulz, C., Kramer, H., Zhao, H. and Damiano, L. (2000). Innovative ultra-low NOx controlled auto-ignition combustion process for gasoline engines: The 4-SPACE project. *SAE Paper No.* 2000-01-1873.

Li, J., Zhao, H. and Ladommatos, N. (2001). Research and development of controlled auto-ignition (CAI) combustion in a 4-stroke multi-cylinder gasoline engine. *SAE Paper No.* 2001-01-3608.

Li, Y., Zhao, H., Brouzos, N. and Ma, T. (2006). Effect of injection timing on mixture and CAI combustion in a GDI engine with an air-assisted injector. *SAE Paper No.* 2006-01-0206.

Nicholls, J. A. (1972). *Stream and Droplet Breakup by Shock Waves.* NASA SP-194 (Eds. D.T. Harrje and F.H. Reardon). 126–128.

Ranz, W. E. and Marshall, W. R. (1952). Evaporation from drops-Part I and II, *Chem. Eng. Prog.* **48**, **3**, 141.

Reitz, R. D. and Diwakar, R. (1986). Effect of drop breakup on fuel sprays. *SAE Paper No.* 860469.

Sato, S., Kweon, S. P., Yamashita, D. and Iida, N. (2006). Influence of the mixing ration of double componential fuel on HCCI combustion. *Int. J. Automotive Technology* **7**, **3**, 251–259.

Weltens, H. (1993) Optimization of catalytic gas flow distribution by CFD prediction. *SAE Paper No.* 930784.

Yuen, M. C. and Chen, L. W. (1976). On drag of evaporating liquid droplets. *Combust. Sci. and Tech.* **14**, 147–154.